Heliyon 6 (2020) e05772

Contents lists available at ScienceDirect

Heliyon

journal homepage: www.cell.com/heliyon

Research article

Proposal of an open-source computational toolbox for solving PDEs in the context of chemical reaction engineering using FEniCS and complementary components

Santiago Ortiz-Laverde [a], Camilo Rengifo [b], Martha Cobo [a], Manuel Figueredo [a,*]

[a] Energy, Materials and Environment Laboratory, Department of Chemical Engineering, Universidad de La Sabana, Campus Universitario Puente del Común, Km. 7 Autopista Norte, Bogotá, Colombia

[b] Department of Mathematics, Physics and Statistics, Universidad de La Sabana, Campus Universitario Puente del Común, Km. 7 Autopista Norte, Bogotá, Colombia

ARTICLE INFO

Keywords:
Aspen custom modeler
Chemical engineering
FEniCS
Open-source computational toolbox
o-xylene oxidation
Power-to-methane

ABSTRACT

In this contribution, an open-source computational toolbox composed of FEniCS and complementary packages is introduced to the chemical and process engineering field by addressing two case studies. First, the oxidation of o-xylene to phthalic anhydride is modelled and used as a FEniCS′ proof-of-concept based on a comparison with the software Aspen Custom Modeler (ACM). The results show a maximum absolute error of 2% and thus a good FEniCS/ACM agreement. Second, synthetic natural gas (SNG) production through CO_2 methanation is covered in further detail. In this instance, a parametric study is performed for a tube bundle fixed-bed reactor employing a two-dimensional and transient pseudo-homogeneous model. An operating window for critical variables is evaluated, discussed, and successfully contrasted with the literature. Therefore, the computational toolbox methodology and the consistency of the results are validated, strengthening FEniCS and complements as an interesting alternative to solve mathematical models concerning chemical reaction engineering.

1. Introduction

Computational tools have been evolving considerably, allowing engineers to support their designs not only based on heuristics, but also on increasingly complex calculations. Thus, many software and computing environments have been developed to address distinct engineering problems for industrial applications and research purposes. Mathematical modelling, in which both space and time are described based on conservation laws, is expected to improve prediction accuracy since it provides detailed information about the system behaviour and helps engineers in the prototyping process during the early development stages (Ferziger and Perić, 2002; Gustafsson, 2011). Thus, software with solvers capable of computing partial differential equations (PDEs) is required. Nonetheless, most are expensive and hardly accessible to the industry or academic community, leading to an increasing interest in out-of-the-box open-source computational tools.

In this research, FEniCS, Gmsh, ParaView and some Python libraries (e.g., pygmsh, meshio, NumPy, matplotlib and vedo) are employed to perform the computing, mesh generation and data post-processing tasks. The FEniCS Project is a novel open-source computing platform for the automated solution of PDE sets using the finite element method (FEM). It offers high-level scripting by employing Python as the programming language, which enables not only flexibility but also an efficient, streamlined FEM implementation (Alnæs et al., 2015; Logg et al., 2012; Logg and Wells, 2010). Gmsh is an actively maintained finite element meshing framework with a built-in CAD engine and a user interface with advanced visualization capabilities (Geuzaine and Remacle, 2009). ParaView is a well-known software in computer science for post-processing and visualization applications. It provides cutting edge tools to inspect and analyse data both qualitatively and quantitatively (Ahrens et al., 2005; Ayachit, 2015).

The FEniCS Project has been used within a wide range of research fields, such as tidal energy, geoscience, fluid mechanics, theoretical biology, strain gradient elasticity, biophysics and metamodelling (Abali, 2019; Epanchintsev et al., 2016; Funke et al., 2019; Goodwin et al., 2019; Haagenson et al., 2020; Janečka et al., 2019; Lejeune, 2020; Murray and Young, 2020; Phunpeng and Baiz, 2015; Zhu and Yan, 2019). Abali (2017), for instance, demonstrated several modelling examples with different engineering applications through a continuum mechanics approach. However, there is currently no literature concerning its

* Corresponding author.
E-mail address: manuel.figueredo@unisabana.edu.co (M. Figueredo).

https://doi.org/10.1016/j.heliyon.2020.e05772
Received 15 July 2020; Received in revised form 27 October 2020; Accepted 15 December 2020

application in chemical and process engineering. This paper aims to introduce FEniCS and the complementary components as an open-source computational toolbox to solve standard chemical reaction engineering problems for research or educational purposes. To accomplish the latter, two case studies are proposed and solved.

The first case study consists of a fixed-bed reactor simulation for the selective oxidation of *o*-xylene to phthalic anhydride catalysed by V_2O_5/TiO_2. This has been a recognized heterogeneous catalytic process within the petrochemical industry (Bünger, 1988) and the subject of several studies looking for enhanced catalyst and reaction technologies due to the existing risk of thermal runaways (Calderbank et al., 1977; Dias et al., 1995; Gimeno et al., 2008; Herten and Froment, 1968; Papageorgiou et al., 1994; Skrzypek et al., 1985; Vanhove and Blanchard, 1975).

This case study became a landmark example for chemical reactor analysis and design in assessing hot spot formation, as first proposed by Froment et al. (1990). It has also been used to evaluate other process engineering software, as in the case of Oh and Pantelides (1996), who adopted it to illustrate the capability of process modelling languages using the gPROMS framework. It is currently part of the Aspen Custom Modeler (ACM) software documentation as an example in the PDE modelling section (Aspen Technology Inc., 2016).

In fact, ACM is software developed by AspenTech, a company with high recognition in academia and industry, given its background in engineering process modelling, simulation, and optimization. Therefore, unlike other open-source platforms/packages that, as well as FEniCS, are intended to solve PDEs, ACM not only provides an environment for computing custom-based PDEs with the desired level of flexibility and sophistication, but is also the only one aimed at modelling and simulating engineering processes. Furthermore, ACM takes advantage of the Aspen properties databases, enabling the export of customized models as process equipment into other featured AspenTech products, such as Aspen Hysys and Aspen Plus.

Accordingly, phthalic anhydride synthesis is a well-known and studied problem and serves as a proof-of-concept case study of FEniCS in the field of chemical and process engineering when comparing the results with the solution computed via ACM. Then, the same reactor dimensions and conditions recorded by Oh and Pantelides (1996) and the ACM documentation were computed using FEniCS.

On the other hand, the second case study is intended to highlight the computational toolbox applicability in a topic of interest to today's scientific community and one of the Energy, Materials, and Environment Laboratory's leading research lines. This case is then the foremost approach of the paper and addresses the catalytic production of synthetic natural gas (SNG). A state-of-the-art research problem immersed in the power-to-methane (P2M) context that has begun to attract significant attention is proposed as a promising strategy to reduce global greenhouse gas (GHG) emissions while allowing low-carbon footprint power generation (Ghaib and Ben-Fares, 2018).

P2M implies the capture of carbon dioxide (CO_2) from distinct GHG sources and its subsequent catalytic transformation (chemically known as methanation) into SNG using water (H_2O) and surplus renewable electricity (e.g., wind, solar, hydro) (Ghaib et al., 2016; Wang et al., 2011). One of the major difficulties concerning CO_2 methanation is appropriate heat management due to its highly exothermic nature. This task becomes more challenging within P2M at the industrial level when intermittency is introduced to the operation, due to the fluctuations in the hydrogen supply chain (water electrolysis powered by renewable energies) (Götz et al., 2016; Rönsch et al., 2016). Some investigations have addressed these challenges in CO_2 methanation by paying attention to the reaction engineering aspects from a modelling and simulation perspective. Table 1 shows an overview of recent studies in reactor modelling in CO_2 methanation, reporting the simulated systems, model complexity, and software and numerical methods thus far employed.

According to Table 1, seventeen studies have assessed the reaction engineering considerations in CO_2 methanation through modelling and simulation. In short, most of them (~88 %) relied on PDE systems, giving

Table 1. Overview of reactor modelling for CO_2 methanation.

Catalytic reactor type	Model nature	Software/Computing environment	Numerical method(s)	Reference
Fixed-bed	Dynamic – 1D (PDE)	CasADi [¶]	FVM	Zimmermann et al. (2020)
Micro packed-bed	Stationary – 1D (ODE)	MATLAB® ode15s	NDFs	Farsi et al. (2020)
Slurry bubble column	Dynamic – 1D (PDE)	MATLAB® ode15s	MOL/NDFs	Lefebvre et al. (2020)
Fluidized-bed	Stationary – 1D (ODE)	MATLAB® ode15s	NDFs	Jia et al. (2020)
Fixed-bed and intensified	Dynamic – 2D (PDE)	CasADi [¶]	FVM	Bremer and Sundmacher (2019)
Micro-structured fixed-bed	Dynamic – 1D (PDE)	gPROMS ModelBuilder	BFD1	Kreitz et al. (2019b)
Catalyst coated on heat exchanger	Stationary – 2D, 3D (PDE)	COMSOL Multyphysics®	FEM	Vidal Vázquez et al. (2018)
Plug flow	Stationary – 1D (ODE), 3D (PDE)	COMSOL Multyphysics®/Ansys®	FEM/FVM	Gruber et al. (2018)
Fixed-bed	Dynamic – 1D, 2D (PDE)	n.s./CasADi [¶]	n.s./FVM	Rätze et al. (2017)
Fixed-bed	Dynamic – 2D (PDE)	CasADi [¶]	FVM	Bremer et al. (2017)
Microchannel	Stationary – 3D (PDE)	COMSOL Multyphysics®	FEM	Engelbrecht et al. (2017)
Fixed-bed	Stationary – 2D (PDE)	COMSOL Multyphysics®	FEM	Ducamp et al. (2017)
Fixed -bed	Dynamic – 1D (PDE)	MATLAB® PDE solver/ode15s	FEM/NDFs	(Sun and Simakov, 2017)
Fixed-bed	Dynamic – 1D (PDE)	MATLAB® PDE solver/ode15s	FEM/NDFs	(Sun et al., 2017)
Fixed-bed	Stationary – 2D (PDE)	COMSOL Multyphysics®	FEM	Chein et al. (2016)
Fixed-bed	Stationary – 1D (ODE), 2D (PDE)	MATLAB® ode15s and bvp4c-s/COMSOL Multyphysics®	NDFs/FEM	Schlereth and Hinrichsen (2014)
Fluidized-bed	Dynamic – 2D (PDE)	OpenFoam	FVM	Liu and Hinrichsen (2014)

Abbreviations at the end of the manuscript. [¶] CasADi framework in MATLAB® (Andersson, 2013). n.s. is not specified.

robustness to mathematical modelling. Almost half (~53 %) considered dynamic models with the notion that methanation reactors need to handle load intermittency and be started up and shut down frequently within the P2M context. Among those, four studies (~23 %) considered two/three-dimensional (2D/3D) spatial distributions aside from transitory effects; in such studies, the finite volume method (FVM) was used. Indeed, Schlereth and Hinrichsen (2014) and Rätze et al. (2017) argued the importance of a radial description of the temperature profile to have a quantitative evaluation rather than a qualitative trend, especially under dynamic reactor operations. Last, only 1 study adopted open-source software to develop the modelling calculations, and Liu and Hinrichsen (2014) performed CFD simulations in OpenFoam to analyse the hydrodynamics and methanation reactions in a fluidized-bed reactor, which shows the lack of employment of open-source tools in the numerical analysis of CO_2 methanation systems.

Therefore, in the second case study FEniCS and complementary open-source tools are employed to address a chemical engineering problem within the P2M context. More precisely, the effect of various operational variables on hot spot formation and CO_2 conversion is evaluated in an average tube bundle fixed-bed reactor through a 2D dynamic model. The obtained results are qualitatively and quantitatively contrasted with the recorded literature to ascertain their reliability, and the analysis contributes to creating the big picture of the parametric sensitivity of the CO_2 methanation process. Together with the first case study, this demonstrates the feasibility of the proposed computational toolbox within a research scenario in the chemical and process engineering fields.

The nomenclature and abbreviations used throughout the text are listed at the end of the manuscript for ease of reading.

2. Computational toolbox and methodology

The two case studies are addressed through a series of sequential steps. The first is to identify the PDEs (PDE set) describing the modelled phenomena, the computational or discretized domain, and the corresponding boundary conditions. Once the former has been established, the second step consists of generating the FEM mesh according to the required accuracy. Then, the mathematical model is reformulated as a finite element variational problem (also known as the weak formulation), followed by a Python program in which the mathematical problem is computed over the discretized domain through FEniCS abstractions. The last step consists of storing the data for post-processing purposes (e.g., visualization). While Gmsh (in-line with pygmsh and meshio) and FEniCS combine the meshing and subsequent FEM application, ParaView (plus certain Python modules) is used for data post-processing. Accordingly, the proposed open-source toolbox and its interoperability are described in more detail in this section.

2.1. Mesh generation

To select an appropriate meshing tool, some of the most commonly used tools were identified without any prior attachment. The decision was based on a review article by Spencer Smith et al. (2016) and the information available within the FEniCS community. In the former, 27 Mesh Generation and Mesh Processing (MGMP) software programs were assessed. Their analysis criteria included software maintainability, usability, reusability, and performance. Although this research is not completely updated, it provides a general review of the available software in the field, their shortcomings, and strengths.

According to this review, the top 5 MGMP projects ranked by quality were CGAL (The CGAL Project, 2020), MeshLab (Cignoni et al., 2008), TetGen (Si, 2013), snappyHexMesh (The OpenFOAM Foundation, 2019) and Gmsh (Geuzaine and Remacle, 2009). All of these methods are open-source and demonstrate surface robustness (appropriate error handling). Regarding operating system portability, CGAL, MeshLab, TetGen and Gmsh may be supported in Windows, Linux and OSX, while snappyHexMesh is only supported in Linux. However, MeshLab and TetGen solely support meshing of triangular and tetrahedral elements for 3D polyhedral-type domains, whereas snappyHexMesh is used mainly as a mesh generator tool for OpenFoam in 3D meshes containing hexahedra and split-hexahedra (where triangulated surface geometries are required as inputs).

On the other hand, both CGAL and Gmsh support 1, 2 and 3D meshes and have been employed as FEniCS external mesh generators. In addition, the user may build customized meshes through native scripting in each software, which is advantageous because it makes the creation of complex geometries more flexible. Notwithstanding, the implementation of Gmsh was found to be easier since there seems to be more information in the community forums concerning Gmsh format treatment and conversion according to feasible FEniCS inputs. Furthermore, the Python package pygmsh enables the creation of finite element meshes through the Python scripting language liaised with the Gmsh API (Schlömer et al., 2020a). The latter makes the creation of Gmsh meshes more versatile and automates the meshing process within the FEniCS computing environment itself. As a result, Gmsh (powered by pygmsh) was incorporated in the proposed computational toolbox as the mesh generation tool. In addition, Gmsh provided an appropriate refinement for triangular meshes over slimline geometries, such as the ones used herein with both case studies.

2.2. FEniCS and the FEM

With high-level Python and C++ as programming languages, FEniCS is a modern collection of open-source software components directed at the automated solution of PDEs via FEM (Alnæs et al., 2015; Logg et al., 2012; Logg and Wells, 2010). One of the distinguishing features of FEM consists of rewriting the mathematical model as a variational problem (also known as weak formulation). To formulate the variational problem, each PDE is multiplied by a function v (called the test function) and integrated over its respective domain, where all the second-order terms are integrated by parts. Eqs. (1), (2), and (3) briefly describe this procedure with a Poisson-like problem, where f accounts for a source term (see Petter Langtangen and Logg (2017)).

$$-\nabla^2 u = f \quad in\ \Omega. \tag{1}$$

$$\int_\Omega (\nabla^2 u) v dx = \oint_{\partial\Omega} v\, \nabla u \ \mathrm{ds} \ - \int_\Omega (\nabla v)\cdot(\nabla u)\, dx\,, \tag{2}$$

$$\mathrm{F}(u;\ v) = \int_\Omega v f\, dx + \oint_{\partial\Omega} v \nabla u \ \mathrm{ds} \ - \int_\Omega (\nabla v)\cdot(\nabla u)\, dx\,. \tag{3}$$

where Ω refers to the physical domain and $\partial\Omega$ refers to the system boundary. Note that the boundary conditions are incorporated in the path integral. In addition, both v and u (trial function to be approximated) are functions that belong to so-called settled function spaces. These spaces of functions consist of piecewise polynomial functions with particular properties in a way that guarantees the continuity of the solution across element boundaries. This research adopts first-order Lagrange polynomials (P1) to approximate the numerical solutions. Once the weak-formulation is stated (e.g., Eq. (1)), a Python program using the corresponding FEniCS abstractions is written. The called solver depends on the nature of the variational problem or whether or not the F statement is linear. The case studies discussed in this paper are nonlinear.

2.3. FEniCS and complements: interoperability

Figure 1 provides a conceptual description of the proposed toolbox interoperability and the following procedure to solve the case studies outlined hereafter. Dotted boxes enclose the respective stages of the computational workflow, while the continuous boxes compose the intercommunication path.

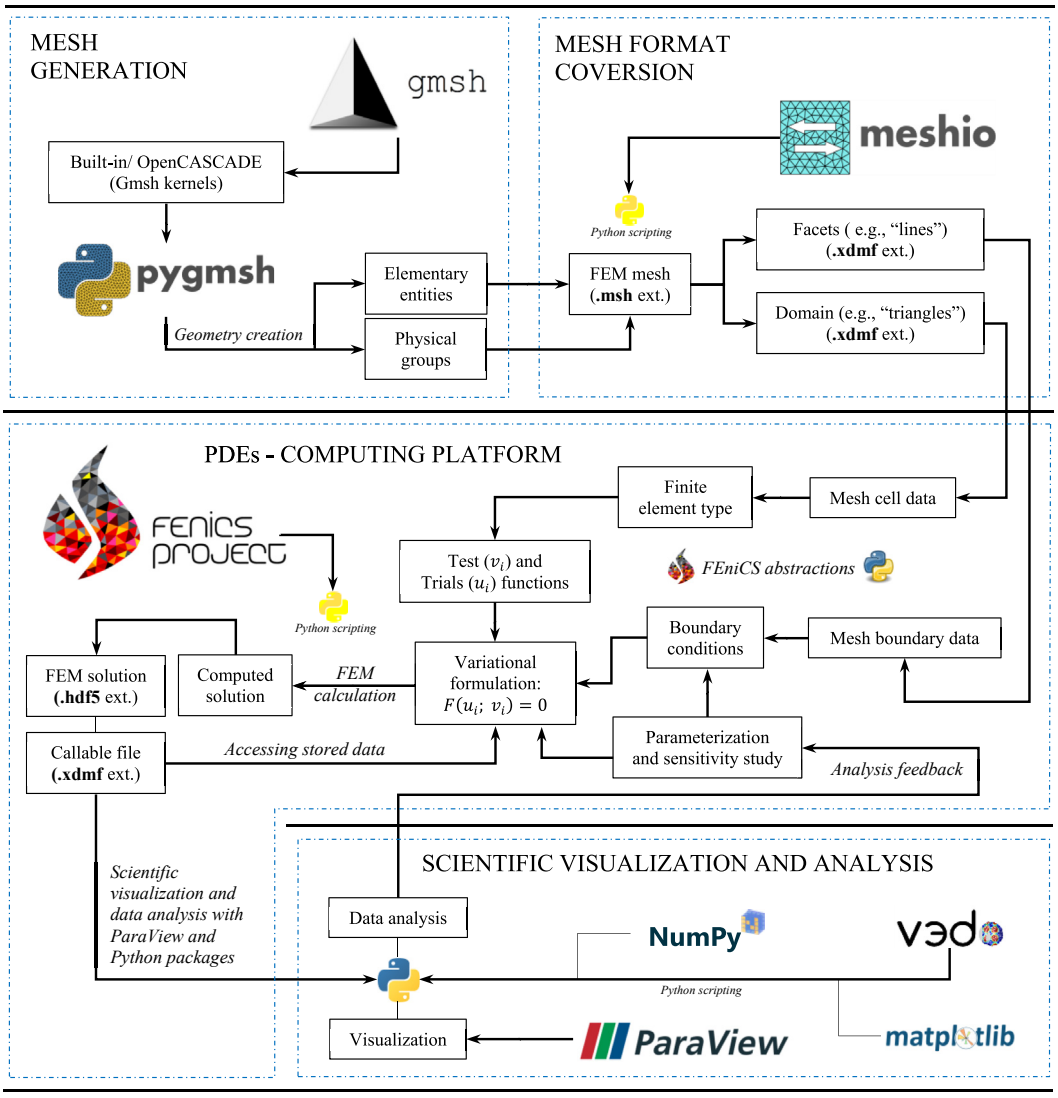

Figure 1. Open-source toolbox interoperability.

By convention, Gmsh uses the *geo* extension (ext.) to create geometric objects before being processed in the mesh refinement. The Python package pygmsh provides an alternative to Gmsh native scripting through a Python interface (Schlömer et al., 2020a). During the creation of geometries (using pygmsh), one may mark specific regions in the geometric object as "physical"; thus, they can be later interpreted as boundaries ($\partial\Omega$) or domains (Ω).

The mesh object created by pygmsh (*.msh* ext.) employing the Gmsh in-house kernels can be converted into formats that support parallel processing. Thus, a preliminary conversion to the XDMF/HDF5 format is required (which is an efficient way to store files both in terms of speed and file sizes) (Camata et al., 2018). It may be accomplished through the Python package meshio since it allows the conversion of *.msh* files (or other ext.) into several formats (Schlömer et al., 2020b). The meshio package splits apart the "physical" and "elementary" entities stored in the *.msh* file so that FEniCS may recognize them before discretization.

After that, test (v_i) and trial (u_i) function spaces are declared based on the type and degree of the selected finite element (polynomial family and order). The latter is followed by the variational formulation statement and the solver setup. Next, the simulation is run, and the results computed by the FEniCS may be stored for visualization or reused later in Python-FEniCS computations. The results are stored in the HDF5 format, which is designed to support I/O parallel operations and is useful for high-performance computing (HPC) (Herbein et al., 2016; Petter Langtangen and Logg, 2017; Soumagne and Biddiscombe, 2011).

The next stage in the workflow is the post-processing of data. Since the entire process is performed through a Python interface, popular libraries for data manipulation and visualization, such as Numpy and matplotlib, or more specialized scientific modules for finite element visualization, such as vedo (formerly known as vtkplotter; Musy et al., 2020, 2019), are available. Regarding external tools, Paraview excels as a proper open-source software for the visualization and analysis of numerical solutions. This tool includes the ability to handle different formats (e.g., VTK, XDMF/HDF5, PVD) and affords a 3D-object interaction environment once the datasets have been imported (Ahrens et al., 2005; Ayachit, 2015). Finally, a parametric sensitivity study is undertaken to obtain information about the mathematical model, with the possibility of

Table 2. Model equations for the phthalic anhydride synthesis reactor.

Description	Mathematical expression	Eq.
Mass balance for component i	$\frac{\partial C_i}{\partial t} = -\vartheta \cdot \vec{\nabla} C_i + \varepsilon D^{eff} (\nabla^2 C_i) + \nu_{i,\,oxy}\, \rho_b\, r_{oxy}$	(4)
Energy balance for packed-bed	$(\rho\, C_p)_{gas} \frac{\partial T}{\partial t} = -\vartheta \cdot \vec{\nabla} T + \lambda^{eff} (\nabla^2 T) + \rho_b (\Delta_R H_{oxy}) r_{oxy}$	(5)
Energy balance for cooling jacket	$(\rho\, C_p)_{cool} \frac{\partial T_{cool}}{\partial t} = (F\, C_p)_{cool} (T_{cool,\,f} - T_{cool}) + (U\ A)_w \int_0^L [T_w(z,\, L) - T_{cool}] dz$	(6)
Boundary conditions for component i	$\varepsilon D_z \frac{\partial C_i}{\partial z}\Big\|_{z=0} = \vartheta_z (C_i - C_{i,\,f})$ $\frac{\partial C_i}{\partial z}\Big\|_{z=L} = 0$ $\frac{\partial C_i}{\partial x}\Big\|_{r=0} = 0$ $\frac{\partial C_i}{\partial x}\Big\|_{r=L} = 0$	(7)
Boundary conditions for the packed-bed Temperature	$\lambda_z \frac{\partial T}{\partial z}\Big\|_{z=0} = (\rho\, C_p)_{gas} \vartheta_z (T - T_f)$ $\frac{\partial T}{\partial z}\Big\|_{z=L} = 0$ $\frac{\partial T}{\partial x}\Big\|_{r=0} = 0$ $\lambda_x \frac{\partial T}{\partial x}\Big\|_{r=L} = U_w (T_{cool} - T)$	(8)

Table 3. Information on numerical methods for case study 1 (using ACM and FEniCS).

Computing platform	Finite elements		Numerical discretization		
	Type	Number of nodes	Axial	Radial	Temporal
FEniCS	Triangular	101040	FEM		BFD1
ACM	Quadrilaterals	12010	BFD1	OCFE3	MOL

being permanently fed back from the same analysed data after each simulation.

2.4. Case studies

2.4.1. Phthalic anhydride synthesis

2.4.1.1. Reactor model description. At the industrial scale, the selective oxidation of *o*-xylene to phthalic anhydride has been mostly conducted in multi-tubular fixed-bed reactors, composed of approximately 2500–20000 parallel tubes (each 3 m long, with an internal diameter of 2.54 cm) and cooled through circulating molten salts (Froment et al., 2011). Herein, only a single of those packed-bed tubes was considered. The resulting equations for a 2D pseudo-homogeneous model are presented in Table 2. The total heat exchanged with the cooling jacket is expressed as an integral over the entire tube length (see Eq. (6)). Danckwerts-type boundary conditions were applied at the entrance of the reactor, whereas the initial conditions for compositions and bed/coolant temperature were set to zero and 625 K, respectively. The catalytic rate model for V_2O_5 was assumed to be first-order with respect to each reagent, despite the presence of an excess of oxygen during the gas-phase air oxidation of o-xylene (Oh and Pantelides, 1996). The physical properties remained constant over the range of the process operating conditions and are given in the supplementary material.

2.4.1.2. ACM and FEniCS numerical procedure. This case study was solved in line with the solution methodology previously described. Gmsh (powered by pygmsh) was used to mesh the reactor domain, and the corresponding variational problem was formulated for Eqs. (4) and (5) and tied down to Eqs. (7) and (8). Additionally, the same mathematical model was implemented in ACM to validate the FEniCS computation. Two numerical methods discretized the spatial domain in the ACM: a 1st-order backward finite difference (BFD1) was applied to the axial coordinate, and a 3rd-order orthogonal collocation on finite elements (OCFE3) was settled along the radial distribution. Regarding the temporal dimension, a simple BFD1 discretization was acceptable in FEniCS while providing stability to the system. In contrast, ACM employs the Method of Lines (MOL) for dynamic- and spatial-distributed problems.

As a result, the discretized domain in the ACM was formed by quadrilateral elements, unlike the triangular mesh used in FEniCS. This discrepancy hinders the numerical comparison of the results. Therefore, once the PDE set was solved in FEniCS, the triangular mesh was squared to a matrix of the same shape as the ACM quadrangular mesh (made of 12010 elements). Likewise, the pygmsh mesh was sufficiently refined with 101040 triangular elements to minimize additional errors due to the comparison process, so the nodes within each new square element could be averaged. Table 3 presents the aforementioned numerical information for both computing platforms.

To facilitate the replication of results concerning this case study and an expanded understanding of the toolbox scheme shown in Figure 1, the detailed variational formulation is given in the Supplementary Material along with some results, and the FEniCS/ACM source codes are provided as Research Data, made available online for academic and non-commercial use at a public repository on GitHub.

2.4.2. Catalytic production of synthetic natural gas (SNG)

2.4.2.1. System description. The CO_2 methanation (Eq. (9)), also referred to as the Sabatier reaction, is a strongly exothermic reaction; therefore, the catalytic systems in which it is held have been designed to avoid excessive overheating. Cooled tube bundle systems are the most commonly used systems for the methanation process (Ghaib et al., 2016; Ghaib and Ben-Fares, 2018; Rönsch et al., 2016). These reactors are composed of heat exchangers and reacting tubes of relatively small diameters (2–5 cm) placed in parallel, which favours heat dissipation and ease of temperature

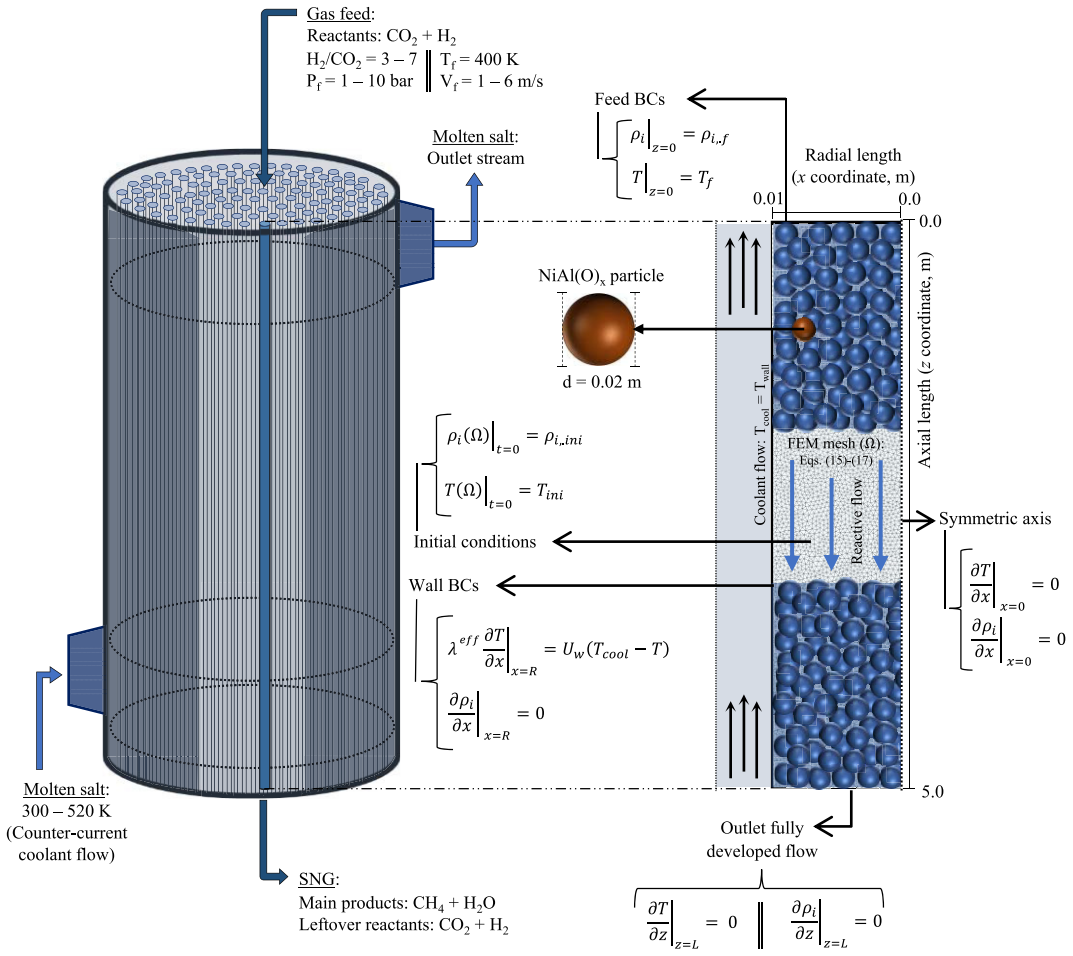

Figure 2. Schematic diagram of the tube bundle fixed-bed reactor packed with spherical NiAl(O)$_x$ for CO_2 methanation.

Table 4. Summary of governing equations for the CO_2 methanation reactor (pseudo-homogeneous approach).

Description	Mathematical expression	Eq.
Species continuity equation	$\varepsilon\frac{\partial \rho_i}{\partial t} = -\vartheta\cdot\vec{\nabla}\rho_i + D_i^{eff}(\nabla^2\rho_i) + (1-\varepsilon)M_i\,\nu_{i\text{-}Sab}\,r_{Sab}^{eff}$	(15)
Energy equation	$(\rho C_p)_{gas}^{eff}\frac{\partial T}{\partial t} = -\sum_i(\rho_i C_{p_i})\vartheta\cdot\vec{\nabla}T + \lambda^{eff}(\nabla^2 T) - (1-\varepsilon)(\Delta_R H_{Sab})r_{Sab}^{eff}$	(16)
Ergun equation	$\frac{dp}{dz} = -150\frac{(1-\varepsilon)^2\mu_{gas}}{d_p{}^2\varepsilon^3}\vartheta_z - 1.75\frac{(1-\varepsilon)\rho_{gas}}{d_p\varepsilon^3}\vartheta_z{}^2$	(17)
Boundary and initial conditions for component i	$\rho_i\|_{z=0} = \rho_{i,f}$; $\frac{\partial \rho_i}{\partial z}\Big\|_{z=L} = 0$; $\frac{\partial \rho_i}{\partial x}\Big\|_{x=R} = 0$; $\frac{\partial \rho_i}{\partial x}\Big\|_{x=0} = 0$; $\rho_i(\Omega)\|_{t=0} = \rho_{i,ini}$	(18)
Boundary and initial conditions for the packed-bed Temperature	$T\|_{z=0} = T_f$; $\frac{\partial T}{\partial z}\Big\|_{z=L} = 0$; $\frac{\partial T}{\partial x}\Big\|_{x=0} = 0$; $\lambda^{eff}\frac{\partial T}{\partial x}\Big\|_{x=R} = U_w(T_{Cool} - T)$; $T(\Omega)\|_{t=0} = T_{ini}$	(19)

management (Eigenberger and Ruppel, 2012; El Sibai et al., 2015). Accordingly, to analyse a reasonable case study at the industrial scale within the P2M context, this paper reproduces the same dimensions evaluated previously in (Bremer et al., 2017; Bremer and Sundmacher, 2019), as well as some other parameters (e.g., catalyst bed porosity (ε) and cooling jacket values). It is assumed that all tubes within the multi-tubular reactor present the same behaviour, and thus only one channel is modelled. The simulated system is shown in Figure 2, and some reactor and catalyst parameters are given in the Supplementary Material.

$$CO_2 + 4H_2 \Leftrightarrow CH_4 + 2H_2O,\ \Delta H_R^{298K} = -164.9\ KJ\ mol^{-1} \quad (9)$$

2.4.2.2. Governing equations and model assumptions. A transient, pseudo-homogeneous mathematical model was employed to simulate the reactor operation. The reacting flow modelling for the methanation process results from the coupling of governing mass, heat, and flow transport phenomena. Herein, the gradient operator $\vec{\nabla}$ accounts for the vector

Table 5. Variational formulation for the governing equations (see Table 4).

Description	Mathematical expression	Eq.
V.F. for species mass-transport Eq. (15)	$\mathrm{F}_i^{n+1}(\rho_i;\, v_i) = \int_\Omega \varepsilon\left(\frac{\rho_i^{n+1}-\rho_i^n}{\Delta t}\right) v_i\, d\mathbf{x} + (\boldsymbol{\vartheta}\cdot\vec{\nabla}\rho_i)^{n+1} v_i\, d\mathbf{x} - \int_\Omega (1-\varepsilon)(M_i\, \nu_{i,sa}\, r_{Sab}^{eff})^{n+1} v_i\, d\mathbf{x} + \int_\Omega (D_i^{eff}(\vec{\nabla}\rho_i\cdot\vec{\nabla}v_i))^{n+1} d\mathbf{x}$	(23)
V.F. for the energy-transport Eq. (16)	$\mathrm{F}_T^{n+1}(T;\, v_T) = \int_\Omega [(\rho C_p)_{gas}^{eff}]^{n+1}\left(\frac{T^{n+1}-T^n}{\Delta t}\right) v_T\, d\mathbf{x} + \int_\Omega \left[\sum_i (\rho_i C_{p_i})\boldsymbol{\vartheta}\cdot\vec{\nabla}T\right]^{n+1} v_T\, d\mathbf{x} + \int_\Omega (1-\varepsilon)(\Delta_R H_{Sab}\, r_{Sab}^{eff})^{n+1} v_T\, d\mathbf{x} + \int_\Omega (\lambda^{eff}(\vec{\nabla}T\cdot\vec{\nabla}v_T))^{n+1} d\mathbf{x} - \oint_{\partial\Omega} U_w(T_{cool} - T)\, v_T ds_w$	(24)
V.F. for the Ergun equation Eq. (17)	$\mathrm{F}_p^{n+1}(P;\, v_p) = \int_\Omega \left(\frac{dp}{dz}\right)^{n+1} v_p\, d\mathbf{x} + \int_\Omega \left[150\frac{(1-\varepsilon)^2\mu_{gas}}{d_p{}^2\varepsilon^3}\vartheta_z\right]^{n+1} v_p\, d\mathbf{x} + \int_\Omega \left[1.75\frac{(1-\varepsilon)\rho_{gas}}{d_p\,\varepsilon^3}\vartheta_z{}^2\right]^{n+1} v_p\, d\mathbf{x}$	(25)
Global V.F. statement	$\mathrm{F}^{n+1}(\rho_i;\, T;\, P;\, v) = \sum_i \mathrm{F}_i^{n+1}(\rho_i;\, v_i) + \mathrm{F}_T^{n+1}(T;\, v_T) + \mathrm{F}_P^{n+1}(P;\, v_p)\, in\, \Omega$	(26)

V.F. refers to Variational Formulation.

$\frac{\partial}{\partial x}\hat{i} + \frac{\partial}{\partial z}\hat{j}$, which provides a 2D notation for the model spatial distribution (see Table 4).

Further details on the approaches used for the calculation of the mass ($D_{\cdot i}^{\cdot eff}$) and heat ($\lambda^{\cdot eff}$) dispersion effective coefficients can be found in the Supplementary Material. In addition, the effective volumetric heat capacity and other thermo-physical properties are estimated, as shown in (Bremer et al., 2017). In any case, the temperature-dependent correlations for the heat capacity, thermal conductivity and dynamic viscosity were obtained by polynomial correlations from the VDI Heat Atlas (VDI, 2010). The pressure drop along the axial reactor coordinate was incorporated through the Ergun equation (Eq. (17)), while the multicomponent gas mixture was assumed to follow ideal gas behaviour. Moreover, the governing equations were solved by subjecting to some boundary and initial conditions (BCs) given by Eqs. (18) and (19) in Table 4. No variations were accounted for at the reactor inlet leading to Dirichlet (or first-type) BCs. Likewise, the inlet values were also set as initial conditions, preventing numerical convergence issues during the simulation start-up. A constant wall temperature (justified by high coolant flows) was applied at the reactor wall, resulting in a Robin BC for the temperature distribution, while the effective heat transfer coefficient at the wall was assumed to be uniform and without thermal resistances along the interface. Zero normal gradients in the temperature and species concentration were assumed at the central axis and reactor outlet due to symmetry and full flow development, respectively. Last, the superficial gas velocity (in the coordinate) was corrected based on the molar flow shift that occurs along the reactor, as described by Eq. (20):

$$\vartheta_z = \vartheta_{z,f} C_{gas,f} / C_{gas} \tag{20}$$

2.4.2.3. CO_2 methanation kinetics. The CO_2 methanation (Eq. (9)) may take place together with the endothermic reverse water gas shift (RWGS) and exothermic CO methanation reactions. Nevertheless, it has been shown that the latter two might be negligible under typical CO_2 methanation conditions due to the low amount of CO produced (Bremer and Sundmacher, 2019; Gao et al., 2012; Koschany et al., 2016; Kreitz et al., 2019a). As a result, this case study relies on a state-of-the-art kinetic model proposed by Koschany et al. (2016) for the CO_2 methanation reaction catalysed by NiAl(O)x and evaluated under industrial conditions. The adopted rate model for the CO_2 methanation reaction is of the type LHHW, as shown in Eq. (21):

$$r_{Sab}^{intr}(T;p_i) = \frac{k(T)\, p_{H_2}^{0.5} p_{CO_2}^{0.5}\left(1 - \frac{p_{CH_4} p_{H_2O}^2}{p_{CO_2} p_{H_2}^4 K_{eq}(T)}\right)}{1 + K_{OH}(T)\frac{p_{H_2O}}{p_{H_2}^{0.5}} + K_{H_2}(T) p_{H_2}^{0.5} + K_{mix}(T) p_{CO_2}^{0.5}}. \tag{21}$$

For further details about adsorption and equilibrium constants, as well as parametrization for the catalytic rate model, see the Supplementary Material.

Moreover, the intrinsic reaction rate (Eq. (21)) is constrained by transport limitations that should be considered to estimate the corresponding effective reaction rate. Some studies have shown that interphase (external) transport limitations can be neglected for the size of catalytic pellets (~3 mm) (Simakov and Sheintuch, 2011; Sun et al., 2017), in contrast to intraparticle (internal) diffusion resistances, which are not negligible.

However, the calculation of an effectiveness factor accounting for internal mass-transport limitations brings considerable computational complexity. Hence, to avoid this additional computation time, an effectiveness factor (η) of 0.1 is used, as reported by Wesenberg and Svendsen (2007) and exemplified by Bremer et al. (2017). Eq. (22) relates the effective (computed with governing equations) and intrinsic reaction rates, where ς refers to a conversion factor.

Table 6. Computational resources.

Operating system	Windows Subsystem for Linux
Processor	Intel(R) Xeon(R) CPU E5-1620 v4 @ 3.50 GHz
CPU cores	4 Cores, 8 Logical Processors
Installed physical RAM	32.0 GB
Hard Disk Drive (HDD)	4TB Hard Drive SATA - 5400 RPM 3.5-inch

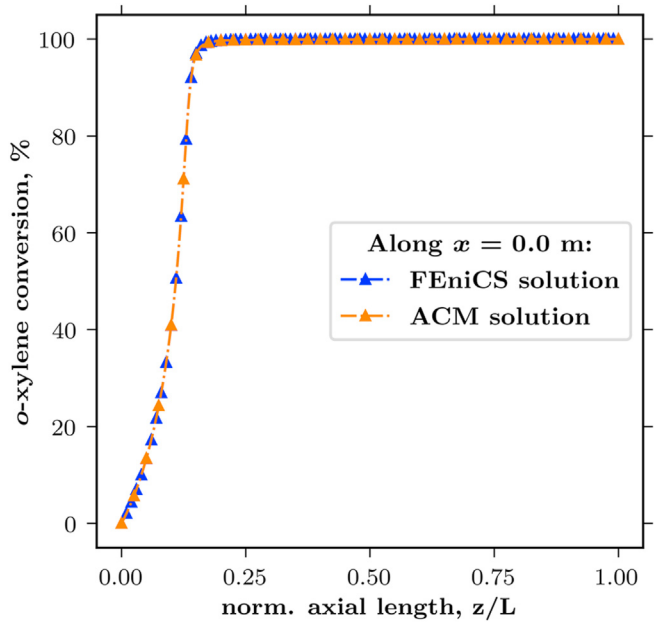

Figure 3. Profiles of the o-xylene conversion obtained using both FEniCS and ACM.

$$r_{Sab}^{eff} = \eta\, \varsigma\, r_{Sab}^{intr}\,. \tag{22}$$

2.4.2.4. Variational formulation. The variational problem concept mentioned in Section 2.2 was applied to Eqs. (15), (16), (17), (18), (19) and the variational formulation for each governing equation is presented in Table 5.

Note that all the time-derivative terms can be approximated by a backward finite difference for simplicity and stability reasons. Additionally, only Robin-type and non-natural Neuman BCs appear in the variational formulation (e.g., Eq. (24)). The remainder (Dirichlet and natural Neuman) vanish but must be applied to the corresponding $\partial\Omega$ in the Python program through a few FEniCS abstractions, which also constrains the FEM solution to those BCs.

2.4.3. Computational aspects

Specifications regarding the computer equipment employed to perform the computations are summarized in Table 6, where no GPU was utilized. The first case study was solved via serial processing despite the fine mesh employed on it, contrary to the second case in which the simulations were run by parallel execution. The reason for this is the numerical complexity exhibited by the set of PDEs in the second case study (despite the coarser mesh used on it), for which grid independence was achieved on up to 8908 triangular elements. Indeed, FEniCS offers flexible parallel computing by partitioning the domain, while the solver computes the solution for each piece separately. This process is accomplished by harnessing the I/O parallel capabilities provided by the XDMF and HDF5 files.

This architecture and FEM setup led to CPU times of less than 1 h and approximately 3 h per simulation for the first and second case studies, respectively. Furthermore, dynamic simulations used 500 steps over the total discrete time in both cases (5 s for the former and approximately 1000–1500 s for the latter). In general, 3D simulations were found to be extremely computationally expensive without further differences in the results from the 2D equivalent cases.

3. Results and discussion

3.1. Case study 1 – phthalic anhydride synthesis

The presence of excess oxygen in the selective oxidation of *o*-xylene to phthalic anhydride causes the reaction rate model to be dependent only on kinetic terms rather than thermodynamics. Then, the oxidation reaction behaves irreversibly with complete conversion as the maximum possible, along with thermal effects within the system of the one-way direction. Moreover, while the conversion presents negligible radial gradients, the temperature profile shows a distinct radial variation due to the formation of a hot spot. Thus, comparing the results from both FEniCS and ACM is acceptable to contrast the conversion profile along the reactor's mid-axis and the temperature over the entire domain. All the contrasting results were retrieved from the last step in the dynamic simulation (stationary state reached). Figure 3 shows the conversion profile in both platforms with a complete conversion near 0.2 (z/L) and a maximum absolute error of ~0.64 %, as defined in Eq. (27).

$$\delta = 100 \cdot \left| \left(n_j^{FEniCS} - n_j^{ACM} \right) \Big/ n_j^{ACM} \right| \tag{27}$$

On the other hand, the fine FEniCS mesh as described in Section 2.4.1.2 was adapted by averaging node values per quadrilateral element to enable a comparison between the 2D distributed profiles. This approach is considered fair enough, as the maximum coefficient of variation (CV) per element in the new quadrangular mesh was below 1% (see Supplementary Material). Figure 4 shows the absolute error between the thermal maps obtained from FEniCS and ACM. This error was

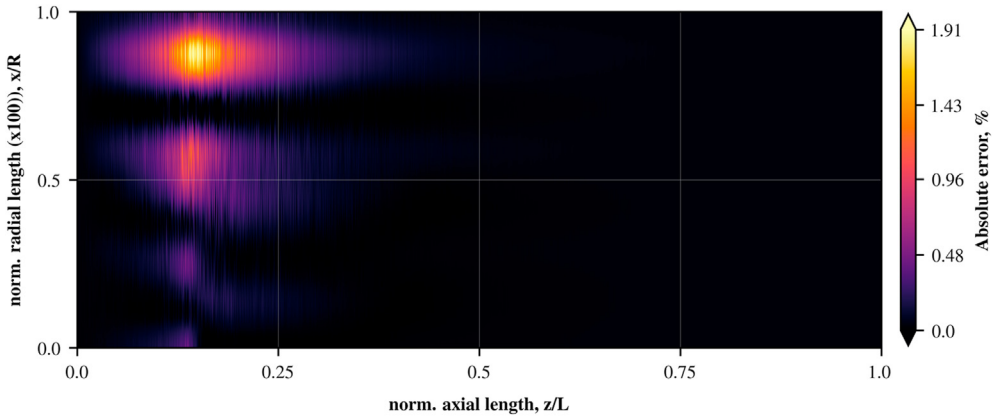

Figure 4. Absolute error for the FEniCS and ACM contrasted thermal maps.

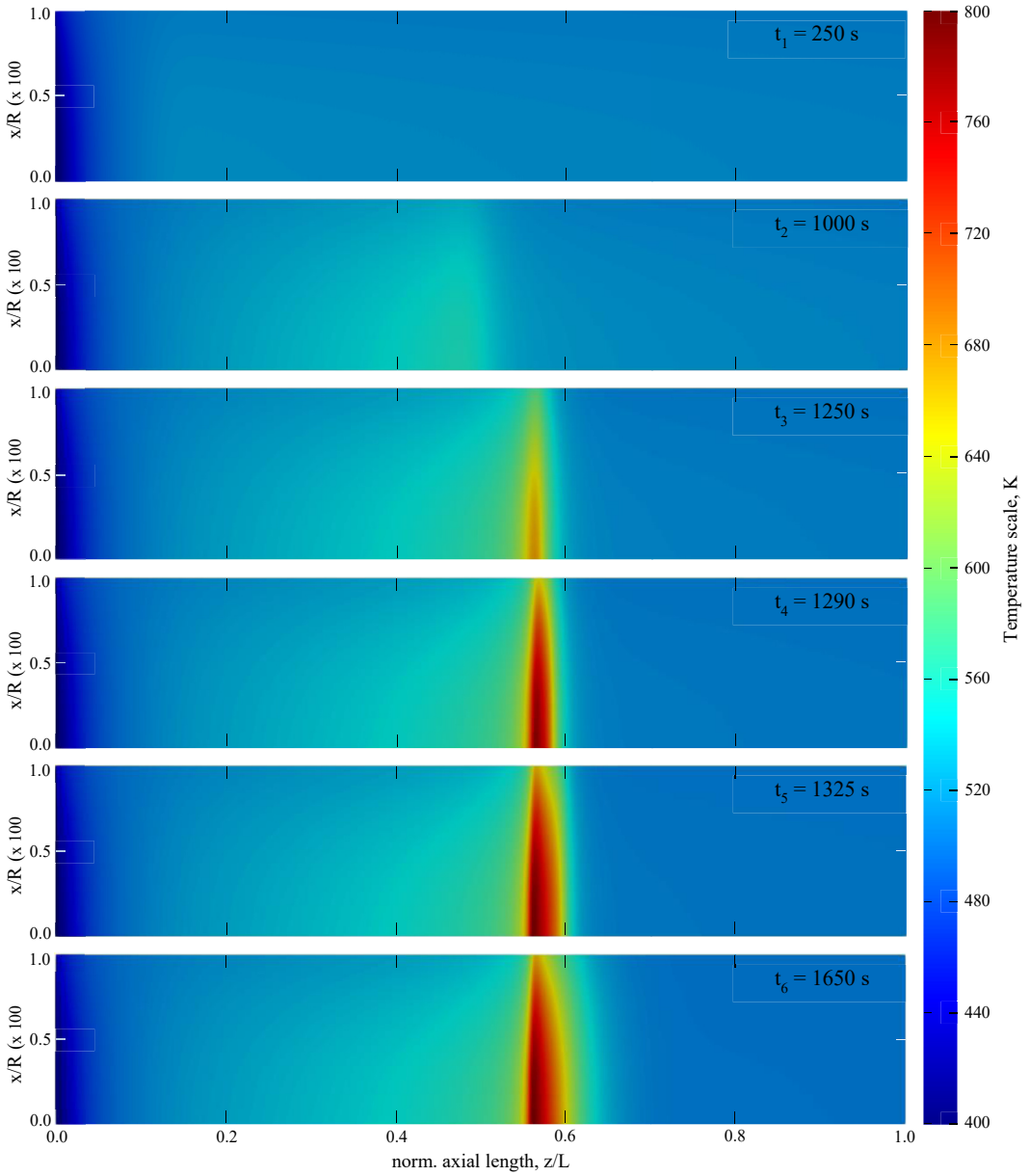

Figure 5. Bed temperature contours along the x-z plane in a single tube of the methanation tube bundle reactor (made with ParaView) from the reactor start-up (t_1 = 250 s) until the steady state (t_6 = 1650 s). This simulation took place with a reactor feed temperature, pressure, gas velocity, and H_2:CO_2 molar ratio of 400 K, 5 bar, 1 m/s, and 4.8, respectively. In addition, the coolant temperature settled at a constant temperature of 500 K.

calculated using Eq. (27) per equivalent node (n_j) over the 2D discretized domain. No error above ~2 % was found, and the most significant differences were contemplated over the hot spot region and particularly in the proximity of the cooling jacket.

The small differences in both the conversion and temperature profiles are due to the varied numerical methods employed in each platform (FEM in FEniCS and BFD1/OCFE3 in ACM). Notwithstanding, a solid consistency was found between the results. Regarding the CPU times, FEniCS performed faster than ACM by a factor of ~1.7, although the triangular mesh employed in FEniCS had ~8 times more finite elements than the ACM quadrangular mesh. It is worth noting that the FEniCS simulations were not executed in parallel, which would undoubtedly further boost their performance in a future scenario.

3.2. Case study 2 – SNG synthesis

The aforementioned mathematical model in Section 2.4.2 was solved exclusively with the proposed computational toolbox due to the large number of equations involved. Therefore, the FEniCS results were solely compared with the literature, where most studies address thermal performance aspects as an inherent feature of CO_2 methanation. The subsequent sections present and discuss the results obtained on the formation of hot spots and overall CO_2 conversion as part of the last stage in the already described workflow (refer to Section 2.3).

3.2.1. CO_2 methanation and reactor hot spots

The heat generated by an exothermic reaction within a fixed-bed reactor operating at a constant wall temperature may eventually overcome the heat removal rate of the cooling jacket, inevitably increasing the temperature in a particular region on what is called a hot spot. The transient evolution of the temperature profile during hot spot formation in the reaction channel is used not only to explain the phenomenon itself, but also to illustrate a dynamic visualization example of the mentioned toolbox components (see Figure 1).

Figure 5 displays the typical thermal map evolution of the packed bed when precise conditions for the Sabatier reaction ignition are given (see

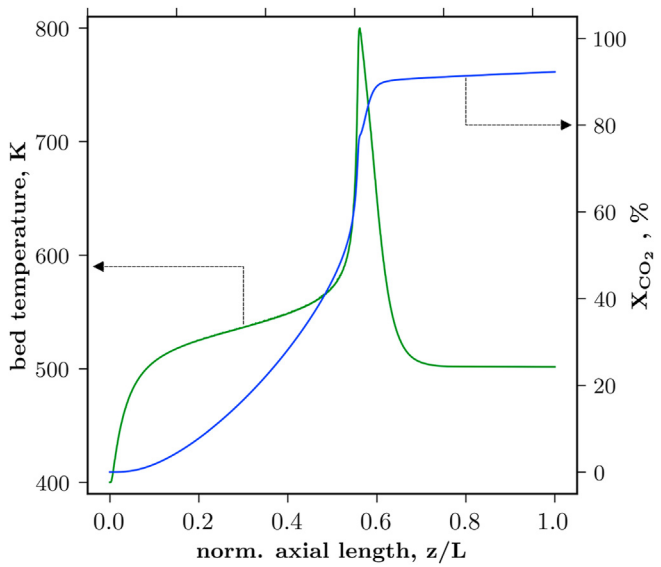

Figure 6. CO_2 conversion and packed-bed temperature profiles along the reactor length (r = 0) at a steady-state (t_6) for the simulation are displayed in Figure 5.

caption), ending with hot spot formation. At the beginning, the reactor is heated due to the difference between the wall and the feed gas temperatures (~t_1). This prior heating makes it easier for the reactants to overcome the kinetic limitations to initiate the methane production. In turn, the advance of the reaction produces additional energy that ultimately leads the system to exceed the wall temperature, at which time the cooling jacket starts removing heat (~t_2).

However, the exponential reaction rate temperature dependence leads the reactants to an ignition state that makes cooling of the jacket insufficient, forming a hot spot up to a length of approximately 2.8 m ($z/L = 0.56$), for this example. The increase in the hot spot's max-temperature is only slowed down by the almost total consumption of the reagents or the emergence of thermodynamic limitations. This indissoluble relationship between temperature and conversion along the fixed-bed reactor is shown in Figure 6. Finally, after approximately 1650 s of operation (~t_6), the system reaches a steady state.

3.2.2. Parametric study variables

One way to validate the results computed by FEniCS and examine the modelled system is to conduct a parametric study. This analysis provides information on the system's sensitivity, whose consistency is discussed, and allows us to establish a correlation with that reported so far. In addition, data analysis from simulations in the parametric study provides feedback to restate the variational problem if reliable results are not entirely achieved and until they are, as indicated in Figure 1.

On this basis, variations in the coolant temperature, inlet gas velocity, feed reactant ratio, and inlet pressure are included. All of them stand as critical process variables that may be subject to unintended load changes or are otherwise operational adjustment variables. To choose the variation range for each critical variable, thermodynamic and kinetic aspects were considered, as well as literature on relevant industrial conditions. Accordingly, all the simulations were run by feeding an undiluted gas mixture of H_2/CO_2 at 400 K as the inlet temperature, whereas the lower and upper range limits for the rest of the process variables are stated in Table 7. For each analysis, one parameter was exclusively ranged within the stipulated limits, while the others remained constant at their respective standard value. The simulations were executed until the system reached a quasi-stationary state (~1000 s depending on the settled conditions).

In the parametric assessment, two key features were assessed: CO_2 conversion and temperature axial distribution. In the case of ignition, the hot spot location, maximum temperature and runaway temperature were discussed. Otherwise, the reaction is said to be either extinguished (overcooled) or just restrained for distinct reasons. Moreover, two targets were established for the bed temperature and CO_2 conversion: for the former, a maximum limit of 775 K, assuming catalyst deactivation (Rönsch et al., 2016; Zimmermann et al., 2020), and for the latter, a tentative minimum CO_2 conversion of 90 %, although it may vary depending on the regional energy quality policies. The conversion for any species was defined as stated in Eq. (28).

$$X_i = 100 \cdot \left[\left(F_i|_f - \left| \sum_j F_i \right|_{z/L=1} \right) \Big/ F_i|_f \right] \tag{28}$$

Although the conversion and bed temperature are generally evaluated as output characteristics, a strictly quantitative correlation with the reported characteristics is rather tricky due to the simultaneous convergence of multiple factors, such as the reactor/cooling system design, the catalytic model employed, and the operating conditions. Notwithstanding, typical patterns derived from the Sabatier reaction thermodynamics were identified and contrasted with the detailed study on methanation thermodynamics developed by Gao et al. (2012). Further quantitative correlations could be established with the analysis conducted by Bremer and Sundmacher (2019) and Zimmermann et al. (2020), given the existence of shared parameters and conditions, whereas qualitative trends could be outlined looking at that recorded elsewhere (refer to Table 1). From here on, the results of the parametric study are presented with pertinent discussions and correlations.

3.2.2.1. Effect of the coolant temperature. First, the parametric sensitivity concerning the cooling temperature was investigated. Figure 7(a) shows that the increase in the cooling temperature favours the conversion of CO_2, where conversions close to equilibrium are reached at coolant temperatures above 500 K. This profile shows a fast ignition curve between 495-500 K caused by the exponential dependence of the reaction rate on the temperature. The results demonstrate how sensitive the reaction system is to the wall (coolant) temperature.

The observed parametric sensitivity is not only due to methanation exothermicity, but also to the high activity of the employed catalyst, as described in the kinetic expression of Koschany et al. (2016). Indeed, this characteristic has also been reported by other studies using the same model (Bremer and Sundmacher, 2019; Gruber et al., 2018; Kreitz et al., 2019b; Zimmermann et al., 2020). Two of them were in fixed-bed reactors, while the remaining were in microstructured reactors. Regarding the former, Bremer and Sundmacher (2019) found an ignition temperature of approximately 465 K, while Zimmermann et al. (2020) reported one up to 515 K. Regardless, it always resulted in CO_2 conversion near the equilibrium curve.

Furthermore, hot spot formation in terms of location and maximum temperature was also investigated. Figure 8(a) shows the bed temperature profile along the reactor normalized length for distinct coolant values. For coolant temperatures between 300 and 490 K (Figure 8(a-

Table 7. Summary of critical variables and their operating limits within the CO_2 methanation reactor.

Process variable	Lower	Upper	Standard	Unit
Coolant temperature	300	530	500	K
Inlet gas velocity	0.5	2	1	m/s
H_2/CO_2 molar ratio	3:1	7:1	4:1	-
Inlet gas pressure	1	10	5	bar

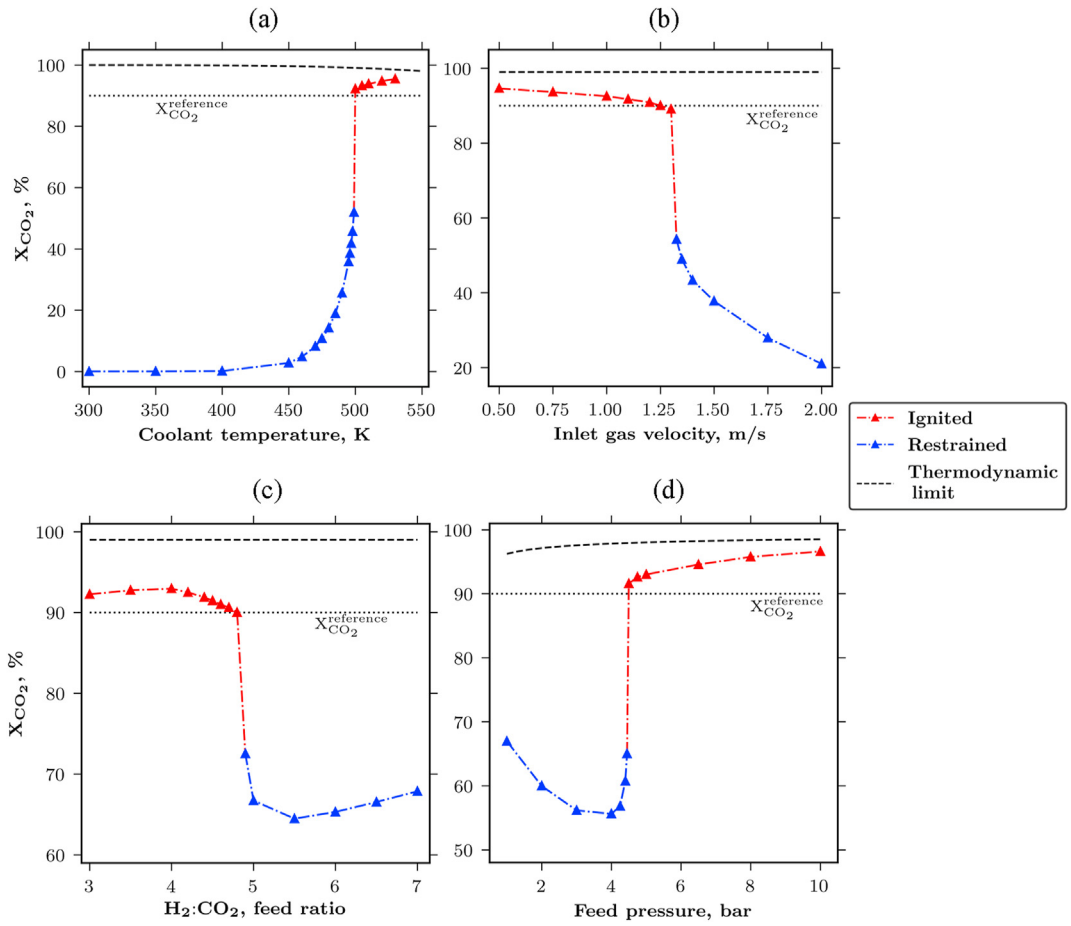

Figure 7. Parametric sensitivity analysis on CO_2 conversion. (a) Effect of the coolant temperature, (b) inlet gas velocity, (c) CO_2:H_2 molar ratio, and (d) feed pressure.

bottom)), the system is forced by heat transfer to reach the boundary (wall) temperature at some point, without any deviation. In contrast, for the range of 490–495 K, a slight bed temperature increment can be appreciated due to low heat accumulation. Last, values equal to or greater than 500 K generate sharp peaks (hot spots) above the established limit target of 775 K, as shown in Figure 8(a-top). For this range, the increase in the wall temperature not only produces a tiny increment in the hot spot maximum temperature but also shows a peak location shift towards the reactor inlet.

The precise hot spot position is difficult to validate, but its maximum temperature has been found in the range of 800–900 K when using the same catalytic model and reactor type (Bremer and Sundmacher, 2019; Zimmermann et al., 2020). Moreover, using a different kinetic model, a parametric study by Schlereth and Hinrichsen (2014) showed a similar trend when evaluating coolant temperature, despite the maximum temperatures exceeding 900 K for that operating case.

3.2.2.2. Effect of the inlet gas velocity. Determining the reactor performance under distinct inlet gas velocities is crucial. This parameter might be subjected to load changes in the P2M context or purposely manipulated to adjust the reactor throughput and the process profitability. Figure 7(b) shows that inlet gas velocities below 1.3 m/s (GHSV = 1560 h^{-1}) result in CO_2 conversions of ~90 % or above, all of which are ignition points. However, slight gains from 1.3 m/s (e.g., 1.325 m/s - GHSV = 1590 h^{-1}) decrease the CO_2 conversions down to ~55 % and beyond to conversions of 20 % for velocities of 2 m/s (GHSV = 2400 h^{-1}).

With the same catalytic model, Zimmermann et al. (2020) reported an equivalent parametric sensitivity for values of ~1 m/s. Deviations shall be related to calculating the transport resistances. In that operating case, a heterogeneous modelling approach was used, rather than the simplified fixed effectiveness factor herein. In addition, using different kinetics, Sun and Simakov (2017) and Sun et al. (2017) exhibited a similar sensitivity for GHSV ranging from 1000-5000 $^{h-1}$.

Moreover, Figure 8(b) shows the temperature profile along the packed bed for different inlet gas velocities. For velocities ≥1.325 m/s, there is a small increase in the maximum bed temperature relative to the coolant temperature (500 K), although this delta remains below ~56 K. In contrast, for lower velocities the presence of steep peaks is evidence of the formation of hot spots. These peaks differ in location and height, which is ascribed to multiple residence times. Decreasing the inlet gas velocity augments the contact/residence time of the reacting flow with the catalyst and diminishes the convective heat transfer, leading to eventual hot spot formation, as would be expected. The observed maximum temperature under the runaway condition is in good agreement with that noticed by Zimmermann et al. (2020) at approximately 840 K.

3.2.2.3. Effect of the CO_2:H_2 molar ratio. In this case, the H_2:CO_2 feed molar ratio was ranged to investigate its effect on CO_2 conversion and hot spot formation from operation start-up. The reagent ratio at the reactor entrance is a critical variable that is likely to undergo fluctuations considering the supply chain in P2M (namely, renewable-powered electrolysis and biogas plants). One way to interpret this variable is to assume a change in the volumetric flow of the reactants supplied separately, maintaining the overall velocity once the mixture is formed.

Figure 7(c) shows a maximum CO_2 conversion (~93 %) for an H_2:CO_2 molar ratio of 4 and the highest parametric sensitivity for molar ratios of approximately 4.9 ± 0.01. The minimum conversion (~64 %) corresponds to a molar ratio of ~5.5, with an increase from that value onwards (up to ~67 %) until 7:1. In addition, the bed temperature in the centreline surpasses the wall temperature for all ratios, as shown in

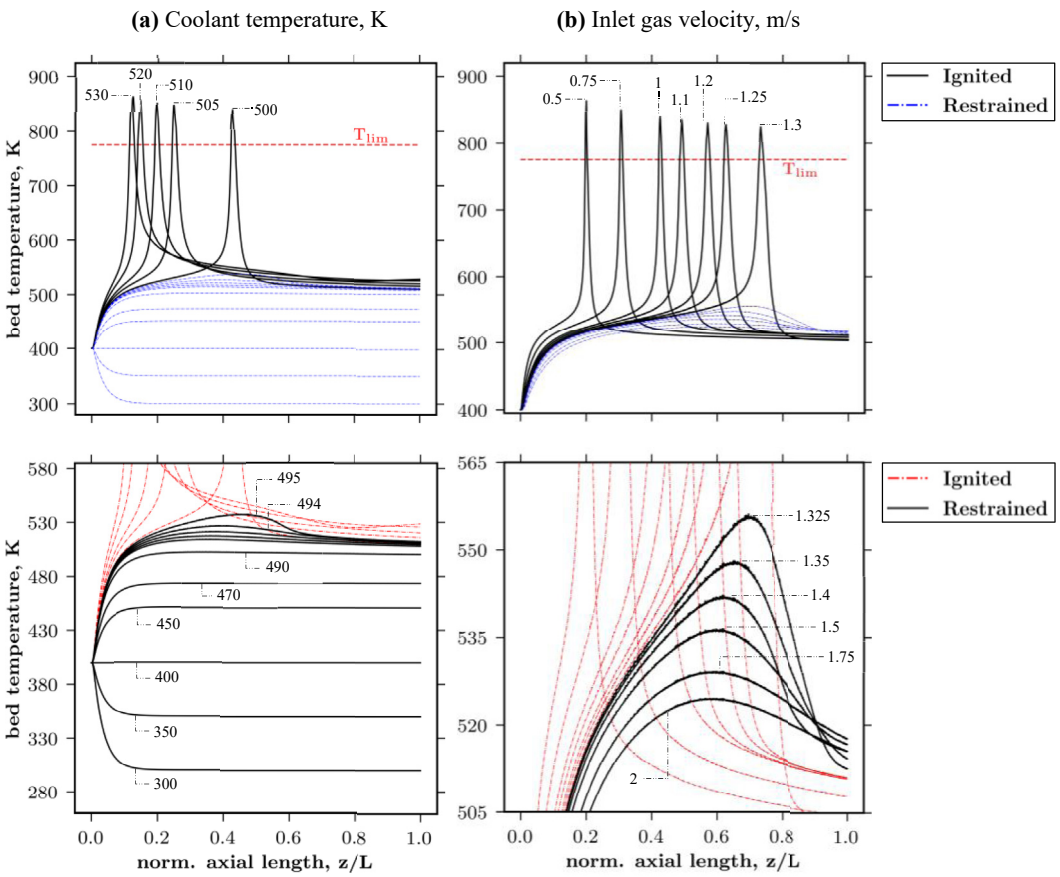

Figure 8. Parametric sensitivity analysis of (a) coolant temperature and (b) inlet gas velocity on the hot spot formation. Black and continuous sharp peaks (top) indicate the presence of hot spots due to ignition conditions, while zoomed continuous black curves (bottom) call for overcooling.

Figure 9(a). Values <4.9 are ignition points for the reaction (top), and the opposite is true for molar ratios ≥4.9.

The effect of the H_2:CO_2 molar ratio on the system is complicated due to the combined interaction of multiple variables, which depend on the gas composition. This effect is outlined for selected variables in the Supplementary Material. Herein, the effective reaction rate was singled as the main rate. The kinetic model by Koschany et al. (2016) shows a maximum rate near a ratio of 4, which may explain the highest conversion achieved under that condition shown in Figure 7(c). However, this is not consistent with the mere thermodynamic study performed by Gao et al. (2012), in which CO_2 conversions increase with the H_2:CO_2 molar ratio up to a value of 6:1. Nevertheless, contrary to the thermodynamic arguments, Kreitz et al. (2019b) also evidenced an inverse relationship between the conversion-molar ratio.

Note that the effective reaction rate is susceptible to other factors outside the gas composition (e.g., temperature, pressure), which suffer multiple variations during dynamic operation and hinder the analysis. The available information about the effect of the molar ratio is fairly nil from a kinetic rather than a thermodynamic perspective. Therefore, additional parametric studies on this variable should be developed to further explore its dynamic effect on reactor performance at the industrial level, beyond the picture outlined here.

3.2.2.4. Effect of the feed pressure. Figure 7(d) shows a complex behaviour concerning the reactor feed pressure and its effect on CO_2 conversion. At low pressures (<~4.4 bar), CO_2 is negatively affected. One reason is that the increase in pressure is associated with an extended injection of reactants, with insufficient conditions to heat the mixture towards an ignition level, and the residence time does not allow for conversions above 70%. Nevertheless, there is an inflection point at approximately 4.4 bar, at which the amount of heat released ignites the system long enough, thus triggering CO_2 conversion. This last circumstance is coupled with the thermodynamic nature of methanation, in which the reaction rate is promoted with absolute pressure. This trend is due to the CO_2 methanation volume reducing behaviour (Gao et al., 2012).

The favouring of pressure in the reaction rate is typical of methanation and has been broadly demonstrated elsewhere (Chein et al., 2016; Ducamp et al., 2017; Engelbrecht et al., 2017; Sun and Simakov, 2017), regardless of the operation case. Furthermore, a quantitative comparison can be established with the parametric analysis conducted by Zimmermann et al. (2020) with acceptable agreement; as observed in Figure 7(d), the same inflection point at 4 bar with conversions between 50-60% and an ignition pressure near 5 bar resulting in CO_2 conversions above 90% were reported therein.

On the other hand, Figure 9(b) shows that feed pressures of 5 bar or above result in ignition states. A slight increment in the maximum hot spot temperature is also observed as the runaway pressure increases. This tendency is ascribed to a higher heat generation relative to an enlarged volume of reagents, which triggers chemical kinetics and raises the bed temperature until the reagents are consumed. The maximum hot spot temperatures are approximately 800–850 K, reasserting the results reported by Zimmermann et al. (2020).

As final remarks, the formation of hot spots is highly susceptible to the investigated inlet process variables (namely, coolant temperature, gas velocity, reagent ratio, and pressure) and is a decisive factor in the attained overall CO_2 conversion. The kinetic component of the reaction rate was observed to prevail over its thermodynamic nature. In any case, for safety reasons an operation should avoid conditions of pronounced parametric sensitivity. Last, the computational toolbox brings a smooth

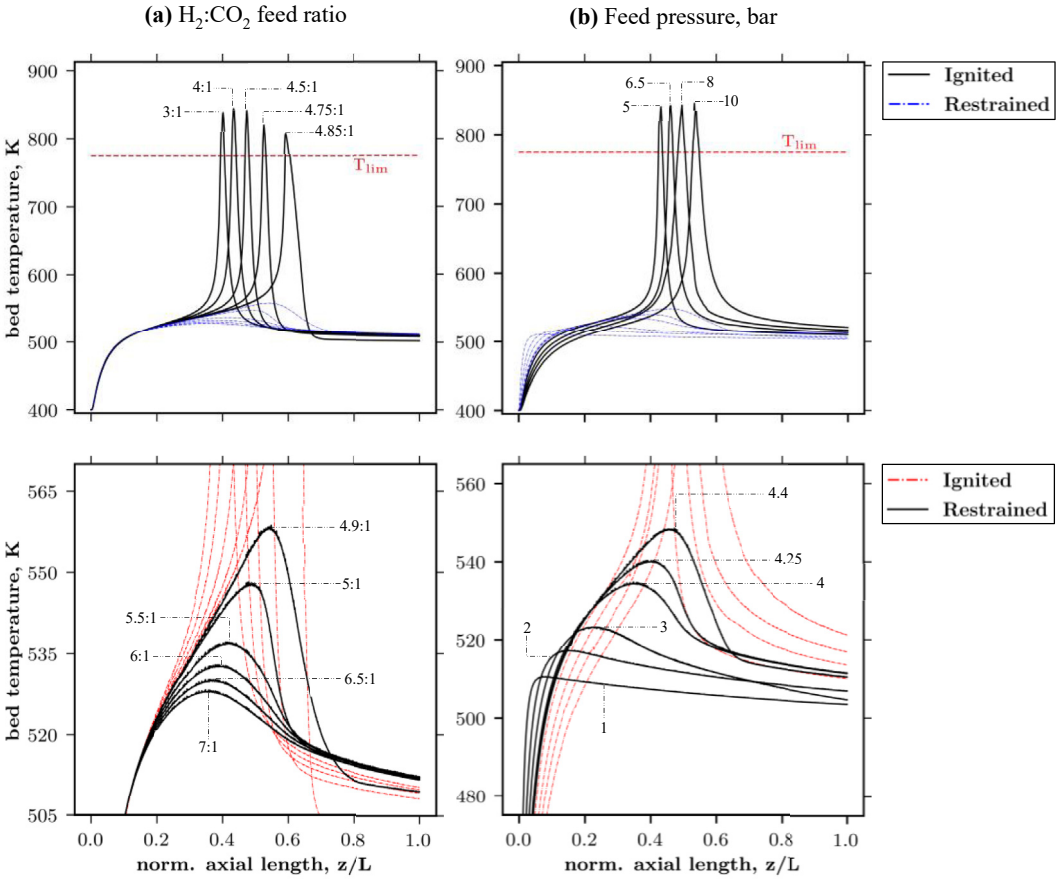

Figure 9. Parametric sensitivity analysis of (a) the feed reagent ratio and (b) pressure on hot spot formation. Black and continuous sharp peaks (top) indicate the presence of hot spots due to ignition conditions, while zoomed continuous black curves (bottom) call for overcooling.

FEM implementation to numerically solve systems of PDEs commonly found in the mathematical modelling of chemical reactors and allows flexible post-simulation data manipulation, enabling, for example, the interpretation of the previously discussed parametric study.

4. Conclusions

In this contribution, a computational toolbox composed of open-source FEniCS and complementary components was employed for the first time in order to solve two case studies in the chemical and process engineering field. Phthalic anhydride production was used as a validation case study, in which the results of FEniCS were contrasted with ACM software. Indeed, an absolute error of up to 2% was recorded after comparing these computational tools. On the other hand, the computational toolbox was used to solve a mathematical model that describes CO_2 methanation in a multi-tubular fixed-bed reactor for industrial P2M applications. The simulations covered an operating window for critical process variables through a parametric study, in which hot spot formation and overall CO_2 conversion were chosen as the response variables. From the analysis, ignition/runaway conditions and the ranges of high parametric sensitivity that should be avoided during reactor operation were identified. The consistency of the results was discussed and compared both qualitatively and quantitatively to varying degrees with those reported so far. The results were reasonable and in harmony with the existing literature, which validates not only the model, but also the reliability of the computational toolbox within a research scenario.

Therefore, FEniCS does serve as a functional computational tool in the chemical and process engineering fields. This toolbox is open-source and gives accurate results, judging by the comparison made with trusted ACM software and the reports in prior research. Hence, it eases access to the scientific and industrial community to address engineering problems. Finally, the application extension of the computational tools exposed above in even more diverse and complex chemical engineering problems is encouraged and required to further test it.

Declarations

Author contribution statement

Santiago Ortiz: Performed the experiments; Analyzed and interpreted the data; Wrote the paper.

Camilo Rengifo & Martha Cobo: Conceived and designed the experiments; Analyzed and interpreted the data; Contributed reagents, materials, analysis tools or data; Wrote the paper.

Manuel Figueredo: Conceived and designed the experiments; Analyzed and interpreted the data; Wrote the paper.

Funding statement

This work was supported by the Colombia Scientific Program within the framework of the call Ecosistema Científico (Contract No. FP44842-218e2018). The authors gratefully acknowledge Universidad de La Sabana for financial support through project ING-208-2018 and the Colombia Scientific Program's funding support within the Ecosistema Científico framework (Contract No. FP44842- 218e2018).

Data availability statement

The ACM and computational toolbox codes for the first case study are made available online for academic and non-commercial use at a public

repository on GitHub. The link to clone the repository is: https://github.com/mafigueredom/RxEngToolbox.

Declaration of interests statement

The authors declare no conflict of interest.

Additional information

Supplementary content related to this article has been published online at https://doi.org/10.1016/j.heliyon.2020.e05772.

Acknowledgements

Santiago Ortiz acknowledges Universidad de La Sabana for the Teaching Assistant Scholarship for his master's studies. The authors are also grateful to the FEniCS community for the technical support provided during the learning curve covered for the proper management of the computational toolbox (this work has no official association with the FEniCS Project). Lastly, D.Sc. Nestor Sánchez is acknowledged for his assistance during the writing.

References

Abali, B.E., 2019. An accurate finite element method for the numerical solution of isothermal and incompressible flow of viscous fluid. Fluid 4, 5.
Abali, B.E., 2017. Computational Reality, Advanced Structured Materials. Springer Singapore, Singapore.
Ahrens, J., Geveci, B., Law, C., 2005. ParaView: an End-User Tool for Large Data Visualization, the Visualization Handbook. Elsevier Inc.
Alnæs, M.S., Blechta, J., Hake, J., Johansson, A., Kehlet, B., Logg, A., Richardson, C., Ring, J., Rognes, M.E., Wells, G.N., 2015. The FEniCS project version 1.5. Arch. Numer. Softw. 3.
Andersson, J., 2013. A General-Purpose Software Framework for Dynamic Optimization (Een Algemene Softwareomgeving Voor Dynamische Optimalisatie).
Aspen Technology Inc., 2016. Aspen Custom Modeler V9.
Ayachit, U., 2015. The ParaView Guide: A Parallel Visualization Application, the ParaView Guide.
Bremer, J., Rätze, K.H.G., Sundmacher, K., 2017. CO 2 methanation: optimal start-up control of a fixed-bed reactor for power-to-gas applications. AIChE J. 63, 23–31.
Bremer, J., Sundmacher, K., 2019. Operation range extension via hot-spot control for catalytic CO 2 methanation reactors. React. Chem. Eng. 4, 1019–1037.
Bünger, H., 1988. Ullmann's encyclopedia of industrial chemistry. In: Dithio-carbamic Acid and Derivates to Ethanol. VCH Verlagsgesellschaft, Weinheim – Deerfield Beach – Basel 1987. XV, 653 S., subskriptionspreis DM 375,–; endgült. Preis DM 465,–, A9, p. 638. Chem. Ing. Tech. 60.
Calderbank, P.H., Chandrasekharan, K., Fumagalli, C., 1977. The prediction of the performance of packed-bed catalytic reactors in the air-oxidation of o-xylene. Chem. Eng. Sci. 32, 1435–1443.
Camata, J.J., Silva, V., Valduriez, P., Mattoso, M., Coutinho, A.L.G.A., 2018. In situ visualization and data analysis for turbidity currents simulation. Comput. Geosci. 110, 23–31.
Chein, R.Y., Chen, W.Y., Yu, C.T., 2016. Numerical simulation of carbon dioxide methanation reaction for synthetic natural gas production in fixed-bed reactors. J. Nat. Gas Sci. Eng. 29, 243–251.
Cignoni, P., Callieri, M., Corsini, M., Dellepiane, M., Ganovelli, F., Ranzuglia, G., 2008. MeshLab: an open-source mesh processing tool. In: Scarano, V., Chiara, R. De, Erra, U. (Eds.), Eurographics Italian Chapter Conference. The Eurographics Association.
Dias, C.R., Portela, M.F., Bond, G.C., 1995. Oxidation of o-xylene to phthalic anhydride over V2O5/TiO2 catalysts. J. Catal. 157, 353–358.
Ducamp, J., Bengaouer, A., Baurens, P., 2017. Modelling and experimental validation of a CO 2 methanation annular cooled fixed-bed reactor exchanger. Can. J. Chem. Eng. 95, 241–252.
Eigenberger, G., Ruppel, W., 2012. Catalytic fixed-bed reactors. In: Ullmann's Encyclopedia of Industrial Chemistry. Wiley-VCH Verlag GmbH & Co. KGaA, Weinheim, Germany.
El Sibai, A., Rihko-Struckmann, L., Sundmacher, K., 2015. Synthetic Methane from CO2: Dynamic Optimization of the Sabatier Process for Power-To-Gas Applications, Computer Aided Chemical Engineering. Elsevier.
Engelbrecht, N., Chiuta, S., Everson, R.C., Neomagus, H.W.J.P., Bessarabov, D.G., 2017. Experimentation and CFD modelling of a microchannel reactor for carbon dioxide methanation. Chem. Eng. J. 313, 847–857.
Epanchintsev, T., Pravdin, S., Sozykin, A., Zverev, V., 2016. Parallel simulation of scroll wave dynamics in the human heart using the FEniCS framework. Procedia Comput. Sci. 101, 68–75.
Farsi, S., Olbrich, W., Pfeifer, P., Dittmeyer, R., 2020. A consecutive methanation scheme for conversion of CO2 – a study on Ni3Fe catalyst in a short-contact time micro packed bed reactor. Chem. Eng. J. 388, 124233.
Ferziger, J.H., Perić, M., 2002. Computational Methods for Fluid Dynamics. Springer Berlin Heidelberg, Berlin, Heidelberg.
Froment, G.F, Bischoff, K.B., De Wilde, J., 1990. Chemical Reactor Analysis and Design. Wiley, New York.
Froment, G.F., Bischoff, B.K., De Wilde, J., 2011. Chemical Reactor Analysis and Design, third ed. Wiley, New York.
Funke, S.W., Nordaas, M., Evju, Ø., Alnæs, M.S., Mardal, K.A., 2019. Variational data assimilation for transient blood flow simulations: cerebral aneurysms as an illustrative example. Int. J. Numer. Method. Biomed. Eng. 35, e3152.
Gao, J., Wang, Y., Ping, Y., Hu, D., Xu, G., Gu, F., Su, F., 2012. A thermodynamic analysis of methanation reactions of carbon oxides for the production of synthetic natural gas. RSC Adv. 2, 2358.
Geuzaine, C., Remacle, J.-F., 2009. Gmsh: a 3-D finite element mesh generator with built-in pre- and post-processing facilities. Int. J. Numer. Methods Eng. 79, 1309–1331.
Ghaib, K., Ben-Fares, F.-Z., 2018. Power-to-Methane: a state-of-the-art review. Renew. Sustain. Energy Rev. 81, 433–446.
Ghaib, K., Nitz, K., Ben-Fares, F.-Z., 2016. Chemical methanation of CO 2: a review. ChemBioEng Rev 3, 266–275.
Gimeno, M.P., Gascón, J., Téllez, C., Herguido, J., Menéndez, M., 2008. Selective oxidation of o-xylene to phthalic anhydride over V2O5/TiO2: kinetic study in a fluidized bed reactor. Chem. Eng. Process. Process Intensif. 47, 1844–1852.
Goodwin, K., Mao, S., Guyomar, T., Miller, E., Radisky, D.C., Košmrlj, A., Nelson, C.M., 2019. Smooth Muscle Differentiation Shapes Domain Branches during Mouse Lung Development. Development 146.
Götz, M., Lefebvre, J., Mörs, F., McDaniel Koch, A., Graf, F., Bajohr, S., Reimert, R., Kolb, T., 2016. Renewable Power-to-Gas: a technological and economic review. Renew. Energy 85, 1371–1390.
Gruber, M., Wieland, C., Habisreuther, P., Trimis, D., Schollenberger, D., Bajohr, S., vonMorstein, O., Schirrmeister, S., 2018. Modeling and design of a catalytic wall reactor for the methanation of carbon dioxide. Chem. Ing. Tech. 90, 615–624.
Gustafsson, B., 2011. Fundamentals of Scientific Computing, Texts in Computational Science and Engineering. Springer Berlin Heidelberg, Berlin, Heidelberg.
Haagenson, R., Rajaram, H., Allen, J., 2020. A generalized poroelastic model using FEniCS with insights into the Noordbergum effect. Comput. Geosci. 135, 104399.
Herbein, S., McDaniel, S., Podhorszki, N., Logan, J., Klasky, S., Taufer, M., 2016. Performance characterization of irregular I/O at the extreme scale. Parallel Comput. 51, 17–36.
Herten, J., Froment, G.F., 1968. Kinetics and product distribution in the oxidation of o-xylene on a vanadium pentoxide catalyst. Ind. Eng. Chem. Process Des. Dev. 7, 516–526.
Janečka, A., Málek, J., Průša, V., Tierra, G., 2019. Numerical scheme for simulation of transient flows of non-Newtonian fluids characterised by a non-monotone relation between the symmetric part of the velocity gradient and the Cauchy stress tensor. Acta Mech. 230, 729–747.
Jia, C., Dai, Y., Yang, Y., Chew, J.W., 2020. A fluidized-bed model for NiMgW-catalyzed CO2 methanation. Particuology 49, 55–64.
Koschany, F., Schlereth, D., Hinrichsen, O., 2016. On the kinetics of the methanation of carbon dioxide on coprecipitated $NiAl(O)_x$. Appl. Catal. B Environ. 181, 504–516.
Kreitz, B., Friedland, J., Güttel, R., Wehinger, G.D., Turek, T., 2019a. Dynamic methanation of CO 2 – effect of concentration forcing. Chem. Ing. Tech. 91, 576–582.
Kreitz, B., Wehinger, G.D., Turek, T., 2019b. Dynamic simulation of the CO2 methanation in a micro-structured fixed-bed reactor. Chem. Eng. Sci. 195, 541–552.
Lefebvre, J., Bajohr, S., Kolb, T., 2020. Modeling of the transient behavior of a slurry bubble column reactor for CO2 methanation, and comparison with a tube bundle reactor. Renew. Energy 151, 118–136.
Lejeune, E., 2020. Mechanical MNIST: a benchmark dataset for mechanical metamodels. Extrem. Mech. Lett. 36, 100659.
Liu, Y., Hinrichsen, O., 2014. CFD simulation of hydrodynamics and methanation reactions in a fluidized-bed reactor for the production of synthetic natural gas. Ind. Eng. Chem. Res. 53, 9348–9356.
Logg, A., Mardal, K.-A., Wells, G.N., others, 2012. Automated Solution of Differential Equations by the Finite Element Method. Springer.
Logg, A., Wells, G.N., 2010. DOLFIN: automated finite element computing. ACM Trans. Math Software 37.
Murray, R., Young, G., 2020. Neutral competition in a deterministically changing environment: revisiting continuum approaches. J. Theor. Biol. 486, 110104.
Musy, M., Dalmasso, G., Sullivan, B., 2019. Marcomusy/Vtkplotter: Vtkplotter.
Musy, M., Jacquenot, G., Dalmasso, G., neoglez, de Bruin, R., Pollack, A., Claudi, F., Badger, C., Icemtel, Sullivan, B., Hrisca, D., Volpatto, D., Zhou, Z.-Q., 2020. marcomusy/vedo: 2020.4.1.
Oh, M., Pantelides, C.C., 1996. A modelling and simulation language for combined lumped and distributed parameter systems. Comput. Chem. Eng. 20, 611–633.
Papageorgiou, J.N., Abello, M.C., Froment, G.F., 1994. Kinetic modeling of the catalytic oxidation of o- xylene over an industrial V2O5-TiO2 (anatase) catalyst. Appl. Catal. Gen. 120, 17–43.
Petter Langtangen, H., Logg, A., 2017. Solving PDEs in Python-The FEniCS Tutorial, I. Springer.
Phunpeng, V., Baiz, P.M., 2015. Mixed finite element formulations for strain-gradient elasticity problems using the FEniCS environment. Finite Elem. Anal. Des. 96, 23–40.
Rätze, K.H.G., Bremer, J., Biegler, L.T., Sundmacher, K., 2017. Physics-Based Surrogate Models for Optimal Control of a CO2 Methanation Reactor, Computer Aided Chemical Engineering. Elsevier Masson SAS.
Rönsch, S., Schneider, J., Matthischke, S., Schlüter, M., Götz, M., Lefebvre, J., Prabhakaran, P., Bajohr, S., 2016. Review on methanation - from fundamentals to current projects. Fuel 166, 276–296.

Schlereth, D., Hinrichsen, O., 2014. A fixed-bed reactor modeling study on the methanation of CO2. Chem. Eng. Res. Des. 92, 702–712.
Schlömer, N., Cervone, A., McBain, G., Tryfon, M.W., Van Staden, R., Gokstorp, F., Toothstone, Dokken, J.S., Anzil, Sanchez, J., Kempf, D., Bussonnier, M., Feng, Y., Awa5114, Maric, T., Chen, S., Nilswagner, Nate, Ivanmultiwave, Fu, F., 2020a. nschloe/pygmsh v6.1.1.
Schlömer, N., McBain, G., Luu, K., Li, T., christos, Ferrándiz, V.M., Barnes, C., Dalcin, L., Eolianoe, nilswagner, Lukeš, V., Gupta, A., Müller, S., Schwarz, L., Blechta, J., Coutinho, C., Beurle, D., Dokken, J.S., S1291, Cereijo, I., Shrimali, B., Cervone, A., Sharma, S., Bussonnier, M., lgiraldi, Jacquenot, G., Vaillant, G.A., Wilson, C., Gudchenko, A.U., Croucher, A., 2020b. nschloe/meshio v4.0.9.
Si, H., 2013. TetGen: A Quality Tetrahedral Mesh Generator and a 3D Delaunay Triangulator. URL. http://tetgen.berlios.vii+97.
Simakov, D.S.A., Sheintuch, M., 2011. Model-based optimization of hydrogen generation by methane steam reforming in autothermal packed-bed membrane reformer. AIChE J. 57, 525–541.
Skrzypek, J., Grzesik, M., Galantowicz, M., Soliński, J., 1985. Kinetics of the catalytic air oxidation of o-xylene over a commercial V2O5-TiO2 catalyst. Chem. Eng. Sci. 40, 611–620.
Soumagne, J., Biddiscombe, J., 2011. Computational steering and parallel online monitoring using RMA through the HDF5 DSM virtual file driver. Procedia Comput. Sci. 4, 479–488.
Spencer Smith, W., Adam Lazzarato, D., Carette, J., 2016. State of the practice for mesh generation and mesh processing software. Adv. Eng. Software 100, 53–71.
Sun, D., Khan, F.M., Simakov, D.S.A., 2017. Heat removal and catalyst deactivation in a Sabatier reactor for chemical fixation of CO_2: simulation-based analysis. Chem. Eng. J. 329, 165–177.
Sun, D., Simakov, D.S.A., 2017. Thermal management of a Sabatier reactor for CO2 conversion into CH4: simulation-based analysis. J. CO2 Util. 21, 368–382.
The CGAL Project, 2020. CGAL User and Reference Manual, 2 ed, 5.0. CGAL Editorial Board.
The OpenFOAM Foundation, 2019. OpenFOAM: User Guide V1219.
Vanhove, D., Blanchard, M., 1975. Catalytic oxidation of o-xylene. J. Catal. 36, 6–10.
VDI, 2010. VDI Heat Atlas, VDI Heat Atlas. Springer Berlin Heidelberg, Berlin, Heidelberg.
Vidal Vázquez, F., Kihlman, J., Mylvaganam, A., Simell, P., Koskinen-Soivi, M.-L., Alopaeus, V., 2018. Modeling of nickel-based hydrotalcite catalyst coated on heat exchanger reactors for CO2 methanation. Chem. Eng. J. 349, 694–707.
Wang, W., Wang, S., Ma, X., Gong, J., 2011. Recent advances in catalytic hydrogenation of carbon dioxide. Chem. Soc. Rev. 40, 3703–3727.
Wesenberg, M.H., Svendsen, H.F., 2007. Mass and heat transfer limitations in a heterogeneous model of a gas-heated steam reformer. Ind. Eng. Chem. Res. 46, 667–676.
Zhu, Q., Yan, J., 2019. A moving-domain CFD solver in FEniCS with applications to tidal turbine simulations in turbulent flows. Comput. Math. Appl.
Zimmermann, R.T., Bremer, J., Sundmacher, K., 2020. Optimal catalyst particle design for flexible fixed-bed CO2 methanation reactors. Chem. Eng. J. 387, 123704.